

Molecular imprinted materials PDA/Fe-MOFs/RGO for the selective and high removal of phenol

Zuchao Meng*, Bin Liu, Mao Li, Xiang Liu, Shanjian Li, Biyun Su

College of Chemistry and Chemical Engineering, Xi'an shiyou University, Xi'an Shaanxi 710065, China, Tel. +(86)029-88382693; emails: zcmeng@xsyu.edu.cn (Z. Meng), 531076535@qq.com (B. Liu), 865381329@qq.com (M. Li), lxhx@xsyu.edu.cn (X. Liu), 690920240@qq.com (S.J. Li), subiyun@xsyu.edu.cn (B. Su)

Received 5 March 2019; Accepted 24 July 2019

ABSTRACT

Molecular imprinting technique is widely applied for molecular recognition in many fields is due to the creation of the recognition sites on a polymer scaffold. The creation of synthetic polymers can specifically recognise template molecules with considerable challenge and potentially rewarding objective. In this work, polydopamine (PDA)/Fe-metal organic framework (MOFs)/reduction graphene oxide (RGO) were prepared by the self-polymerization of dopamine (DA) under mild conditions on the Fe-MOFs/RGO surface. Scanning electron microscopy, Fourier transform infrared (FT-IR) analysis, and transmission electron microscopy were used for the characterization of PDA/Fe-MOFs/RGO. The optimum conditions for the selective and high removal of phenol were studied according to the effects of the dosage of PDA/Fe-MOFs/RGO, pH, initial phenol concentration, contact time and temperature. The results showed that PDA/Fe-MOFs/RGO had high adsorption capacity and good selectivity for the removal of phenol. The adsorption process of phenol onto PDA/Fe-MOFs/RGO was consistent with the pseudo-second-order kinetic model and contained both the surface adsorption and intraparticle diffusion.

Keywords: Metal organic framework; Graphene; Selective adsorption; Phenol; Surface imprinted polymers

1. Introduction

Molecularly imprinted polymers (MIPs) can provide artificial receptor-like recognition sites for template molecules [1,2] and have been widely applied in the separation and purification [3], catalysis [4] and biosensing [5] owing to their high selectivity. The traditional preparation method of MIPs is to dissolve the template molecules, functional monomers, crosslinkers and initiators in a certain proportion in the solvent (pore forming agent). After polymerization, the template molecules are eluted under certain reaction conditions. Although the operation is simple, the resulting MIPs have some problems such as uneven particle size, deep embedding of imprinted molecules, slow mass transfer rate

and poor regeneration effect. Surface molecular imprinting technology overcomes the shortcomings of the traditional preparation method [6]. The recognition sites are built on the surface of the carrier or near the surface [7], which improves the recognition efficiency and binding speed between imprinted polymers and imprinted molecules, and has the advantages of faster adsorption kinetics and higher adsorption capacity [8].

Metal organic framework (MOFs) material is a porous material [9] with periodic network structure formed by metal ions and organic ligands under certain conditions. It has a lot of characteristics, such as large surface area, high porosity, structure order and so on [10]. Su et al. [11] prepared the magnetic $\text{Fe}_3\text{O}_4/\text{SiO}_2/\text{MOF}/\text{TiO}_2$ core-shell nanoparticles,

* Corresponding author.

which showed high adsorption capacity and fast recognition ability for the three azole fungicides in environmental water samples. Qian et al. [12] was used MOF-5 as the imprinted matrix to synthesize a MOF-5@MIP composite with MOF-5 as the matrix, which is under a high adsorption capacity for the template. Liu et al. [13] prepared the MIL-101@MIP core-shell molecular imprinted polymer simply and quickly by one pot polymerization, which had high adsorption capacity and good selectivity for pyrrolidine-3-formic acid. These surface molecular imprinted composites based on MOFs have good stereotactic compatibility with the template molecules on the surface of MOFs, making the template molecules closer to the three-dimensional holes in molecular imprinting, thus showing good selective adsorption properties. At present, there are relatively few reports on the preparation of MIPs on the surface of MOFs. At present, the graphene oxide (GO) has been paid more attention owing to its large specific surface area, chemical stability, abundant pore size distribution [14]. In addition, GO has also the excellent selective adsorption ability through the strong π - π interaction with aromatic compounds containing benzene ring [15]. Hence, GO is a promising adsorbent for removing aromatic compounds in water treatment. The relationship between MOFs and reduction graphene oxide (RGO) might mitigate the poor stability and weak dispersive forces of MOFs [16]. Owing to the favorable attributes of graphene surfaces and high porosity and tunability of MOFs, MOFs/RGO composites were stable and showed high adsorption capacity in the field of adsorption and separation [17,18]. Therefore, the great significance to explore the MIPs based on MOFs/RGO composite.

In this work, polydopamine (PDA)/Fe-MOFs/RGO was prepared by self-polymerization of dopamine (DA) on the Fe-MOFs/RGO surface of the alkaline condition, in which Fe-MOFs/RGO was invoked as the carrier, phenol as a template molecule and DA as a functional monomer. Selective adsorption properties of PDA/Fe-MOFs/RGO for phenol were studied. The results were showed that PDA/Fe-MOFs/RGO had high adsorption capacity and good selectivity for phenol.

2. Experimental setup

2.1. Reagents and characterization

Graphite powder, terephthalic acid, glacial acetic acid and ferric chloride hexahydrate were purchased from Sinopharm Chemical Reagent Co. Ltd. (Shanghai, China). 3-Hydroxytyramine hydrochloride and phenol were obtained from Shanghai Makclin Biochemical Co. Ltd. (Shanghai, China).

UV-vis absorption spectra of phenol were found on a UV-2600 UV-vis spectrophotometer (Shimadzu Corporation, Japan). Scanning electron microscopy (SEM) and energy dispersive spectrum were measured by a scanning electron microscope (JEOL JSM-6700F, Japan). Transmission electron microscopy (TEM) was recorded on a transmission electron microscope (Tecnai G2F20 S-Twin, FEI, USA). Nitrogen adsorption-desorption analysis was done with a specific surface area and porosity analyser (ASAP2020M, China). Fourier transform infrared (FT-IR) spectra were got by a Bruker Vertex 70 FT-IR spectrometer (Bruker Optics, Germany).

2.2. Synthesis of Fe-MOFs/RGO composite

RGO was synthesized by Hummer's method [19]. In brief, in an ice bath, 10 g of graphite powder and 5 g of sodium nitrate were added into the concentrated sulfuric acid to mix evenly and 30 g of KMnO_4 was added while stirring. Then, the mixture was reacted for 30 min at 35°C, and the unreacted potassium permanganate and manganese dioxide were neutralized in 30% of H_2O_2 solution until the color of the mixture changed from brown to bright yellow. Graphite oxide was achieved after filtration and washing. 600 mg of the obtained GO was dispersed in water. GO could be reduced by adding appropriate hydrazine hydrate and stirring for 10 h at 80°C. After filtration and washing, RGO was got.

Fe-MOFs/RGO composite was synthesized according to Jin's method [20]. Briefly, terephthalic acid, iron(III) chloride hexahydrate and acetic acid glacial were mixed uniformly with RGO dispersion. Then the mixture was heated at 150°C for 2 h. Finally, Fe-MOFs/RGO powder can be got at 80°C for 10 h.

2.3. Synthesis of PDA/Fe-MOFs/RGO composite

Solution A was obtained by dissolving 0.165 g of phenol in 40 mL of ethanol. Solution B was got by dissolving 400 mg DA in 360 mL Tris buffer solutions (pH = 8.5). After mixing the solutions A and B, 100 mg of RGO/Fe-MOFs were added. Then the self-polymerization of DA was triggered and maintained at 25°C for 8 h with continuous stirring. After filtrating and eluting with ethanol, PDA/Fe-MOFs/RGO composite was collected, dried at 80°C.

2.4. Effects of adsorption performance

Effects of dosage of PDA/Fe-MOFs/RGO, initial phenol concentration, contact time and other experimental parameters on the adsorption of phenol were investigated. The amount of phenol was adsorbed per unit mass of the adsorbent (q_e) and the removal rate for phenol can be calculated by using the following equations:

$$q_e = \frac{(C_i - C_e)V}{W} \quad (1)$$

$$\text{Removal (\%)} = \frac{(C_i - C_e)}{C_i} \times 100 \quad (2)$$

where C_i is the initial concentration of phenol (mg L^{-1}), C_e is the equilibrium concentration of phenol (mg L^{-1}), V is the volume of solution (L), and W is the mass of adsorbent (g).

2.5. Selective recognition experiments

During the selective recognition of phenol, 20 mg L^{-1} of coexisting compounds (phenol, methylene blue, *p*-nitrophenol, benzoic acid and hydroquinone) were treated. The distribution coefficients (K_d) and selectivity coefficients (k) of methylene blue, *p*-nitrophenol, benzoic acid and hydroquinone with respect to phenol can be obtained depending on the Eqs. (3) and (4) [21].

$$K_d = \frac{Q_e}{C_e} \quad (3)$$

$$k = \frac{K_{d[\text{phenol}]}}{K_{d[X]}} \quad (4)$$

where C_e (mg L^{-1}) represents the equilibrium concentration of each compound and X is the interfering compound.

3. Results and discussion

3.1. Characterization of PDA/Fe-MOFs/RGO composite

3.1.1. Morphological characterization

The morphology of the different products can be observed by SEM and TEM. Fe-MOFs presented octahedral structure (Fig. 1a) and were well grown on two-dimensional RGO nanosheets (Fig. 1b), which were similar to the literature [20]. After the self-polymerization of DA, the surface morphology of Fe-MOFs/RGO changed. The spherical particles were formed, which were suggested by the introduction of PDA

on the surface of Fe-MOFs/RGO (Fig. 1c). Fig. 1c shows the TEM of PDA/Fe-MOFs/RGO, which also indicated PDA/MOF composites were coated on the graphene sheets.

3.1.2. FT-IR spectrum analysis

Fig. 2 shows the FT-IR spectra of different samples at different vibration regions. In the spectra of RGO and Fe-MOFs/RGO, the following characteristic peaks were observed: O–H stretching vibrations ($3,000\text{--}3,500\text{ cm}^{-1}$), C=C stretching or skeletal vibrations from unoxidized graphitic domains (approx. $1,570\text{ cm}^{-1}$), O–H bending vibrations from hydroxyl groups (approx. $1,400\text{ cm}^{-1}$), and alkoxy ($1,052\text{ cm}^{-1}$) [22–24]. The peaks between $1,610$ and $1,292\text{ cm}^{-1}$ are the stretching vibrations of the C=C and the phenolic C–OH stretching vibration of PDA, respectively [25]. An infrared band centered at $1,510\text{ cm}^{-1}$ was from N–H scissoring [26]. Absorption peaks in $3,200\text{--}3,400\text{ cm}^{-1}$ were wider, which was due to the formation of hydrogen bonds between molecules [27]. These results showed that PDA was self-polymerized on the surface of the Fe-MOFs/RGO and PDA/Fe-MOFs/RGO composite was formed.

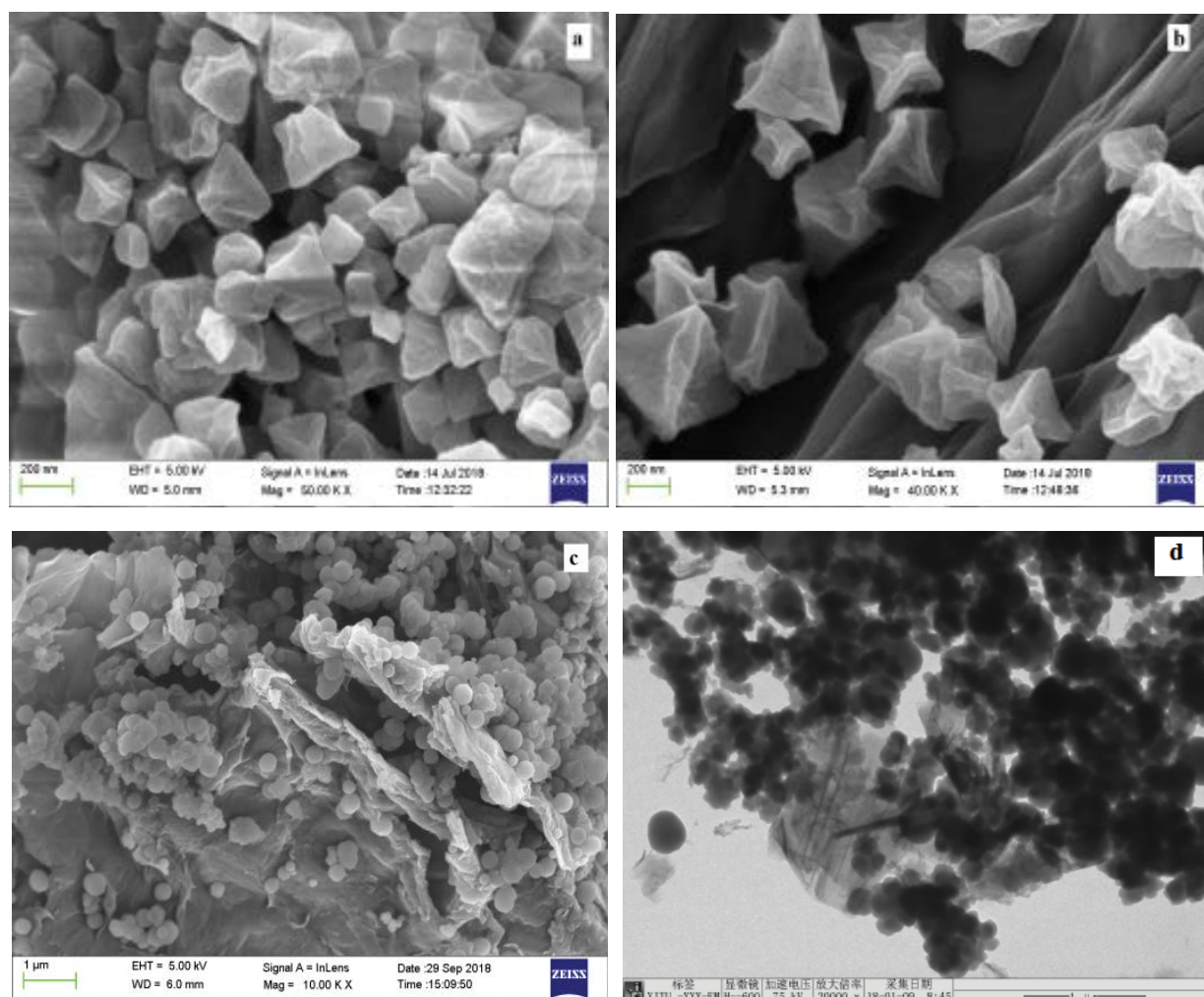


Fig. 1. (a) SEM of Fe-MOFs, (b) Fe-MOFs/RGO, (c) PDA/Fe-MOFs/RGO and (d) TEM of PDA/Fe-MOFs/RGO.

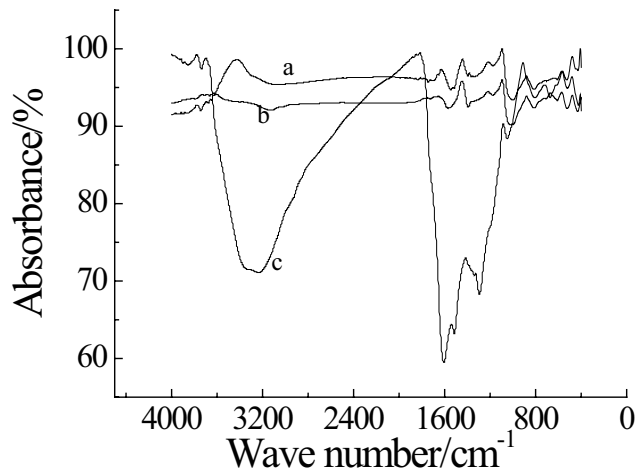


Fig. 2. (a) FT-IR spectrum of RGO, (b) Fe-MOFs/RGO and (c) PDA/Fe-MOFs/RGO.

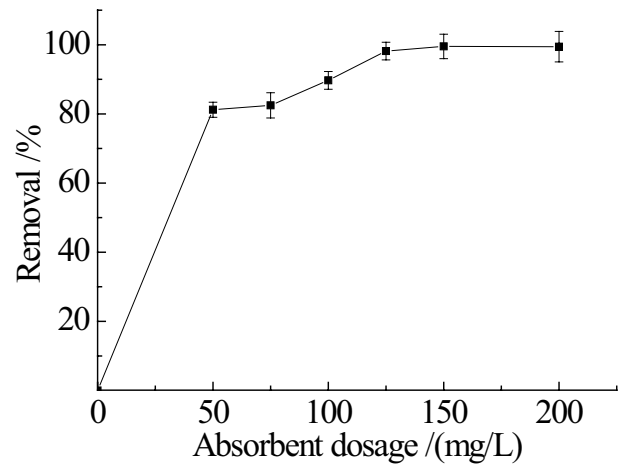


Fig. 3. Effect of adsorbent dose for phenol removal.

3.1.3. Branuett–Emmett–Teller analysis

Table 1 shows the result of Branuett–Emmett–Teller. From Table 1, it can be seen that PDA/Fe-MOFs/RGO had higher pore volume and average pore diameter compared to that of RGO and Fe-MOFs/RGO which helped in providing many channels for the pollutants adsorption and favoured their immigration into the pores [28].

3.2. Effect on adsorption of phenol

3.2.1. Effect of dosage of PDA/Fe-MOFs/RGO

Adsorbent dose is a significant factor to be taken into account for the effective removal of organic pollutant as it can affect the adsorption equilibrium of the system [29]. Different amounts of PDA/Fe-MOFs/RGO were added in 20 mg L⁻¹ phenol solution for 1 h. As shown in Fig. 3, with the increase of PDA/Fe-MOFs/RGO dosage, the removal rate of phenol increased, which can be attributed to the increase of surface area and adsorption site. When the PDA/Fe-MOFs/RGO dosage was more than 125 mg L⁻¹, the effect on the phenol removal rate changed little. So 125 mg L⁻¹ of PDA/Fe-MOFs/RGO was chosen as the dosage of the adsorbent.

3.2.2. Effect of initial concentration of phenol

125 mg L⁻¹ PDA/Fe-MOFs/RGO was added to phenol solution in the range of 8–32 mg L⁻¹ and adsorbed for 1 h. The results are shown in Fig. 4. As shown in Fig. 4, the removal rate of phenol was gradually decreased with the increase of the initial phenol concentration. The reason

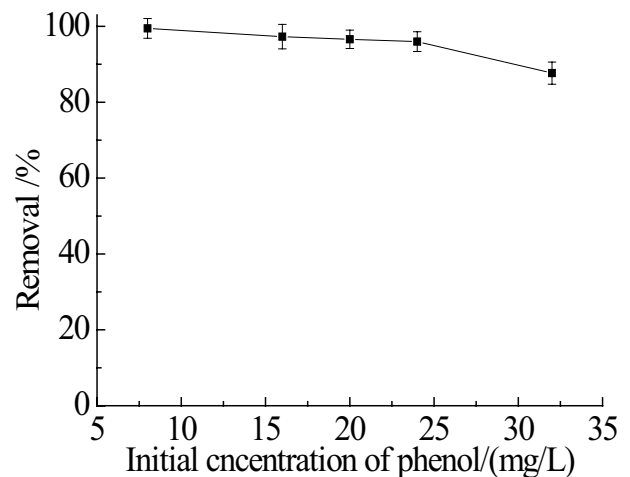


Fig. 4. Effect of initial concentration of phenol for phenol removal.

may be that, most of the original cavities on the surface of PDA/Fe-MOFs/RGO were blocked by the phenol molecules with the increase of phenol concentration, which reduced the number of holes.

3.2.3. Effect of pH

125 mg L⁻¹ of PDA/Fe-MOFs/RGO was added in 20 mg L⁻¹ phenol solutions under different initial pH and adsorbed for 1 h. The results are shown in Fig. 5. It could be concluded that pH had an obvious effect on phenol adsorption. Before

Table 1
Specific surface area, pore volume and pore diameter of the prepared samples

Sample	Pore diameter m/nm	Specific surface area m ² g ⁻¹	Pore volume cm ³ g ⁻¹
RGO	6.53	164.77	0.2691
Fe-MOFs/RGO	7.08	152.93	0.2937
PDA/Fe-MOFs/RGO	10.17	181.93	0.3537

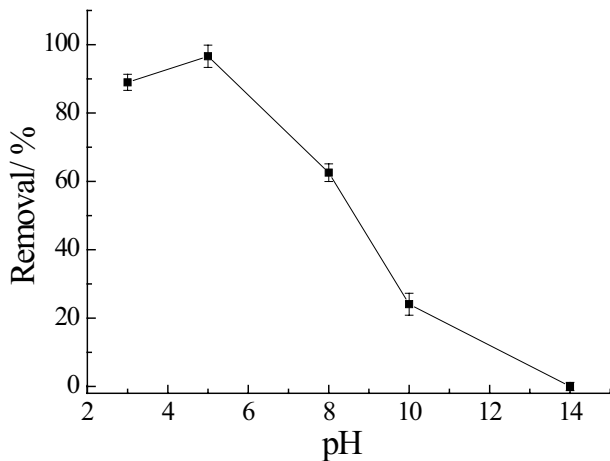


Fig. 5. Effect of pH on removal of phenol on PDA/Fe-MOFs/RGO.

phenol was attached on the surface of PDA/Fe-MOFs/RGO, it had a dissociation process as shown in Eq. (5).



pH values affected the degree of ionization and adsorption of phenol. At a low pH value, PDA/Fe-MOFs/RGO was positively charged due to the protonation of PDA and increased the adsorption of phenolic ions. The pH value is higher than 5, the deprotonation of PDA/Fe-MOFs/RGO made the adsorbents negatively charged, which imposed repulsion with the phenolic ions and was unfavorable for phenol adsorption. So a pH value of 5.0 was established in most appropriate.

3.2.4. Effect of temperature

The removal rate of phenol was influenced by the temperature. As shown in Fig. 6, when temperature was varied in the range of 20°C–60°C, the removal rate of phenol was decreased with the increase of temperature, which may be owing to abating of forces between adsorptive sites of adsorbent and adsorbate [30]. Kilic et al. [31] and Singh et al. [32] was designated the same results for the adsorption of phenol. Therefore, 20°C was selected for additional studies.

3.2.5. Effect of contact time

At 20°C, contact time was affected by the removal of phenol (Fig. 7). From Fig. 7, it can be clearly seen that the removal rate for phenol is increased with increasing contact time. Most of the phenol can be removed in the first 10 min and the equilibrium was reached after 60 min for PDA/Fe-MOFs/RGO, Fe-MOFs/RGO and RGO. Among the three kinds of materials, PDA/Fe-MOFs/RGO showed the highest adsorption rate owing to its large specific surface area and good molecular matching.

3.2.6. Adsorption mechanism and kinetics

The removal of phenol in different phenol solution is shown in Fig. 8. To quantify the changes of phenol adsorption

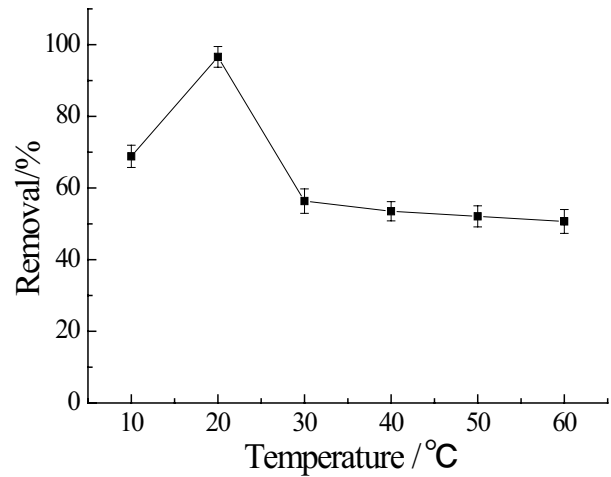


Fig. 6. Effect of temperature on removal of phenol on PDA/Fe-MOFs/RGO.

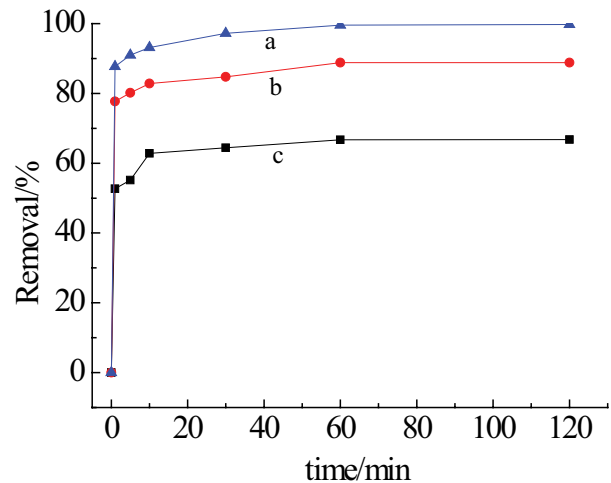


Fig. 7. Removal of phenol on (a) PDA/Fe-MOFs/RGO, (b) Fe-MOFs/RGO and (c) RGO.

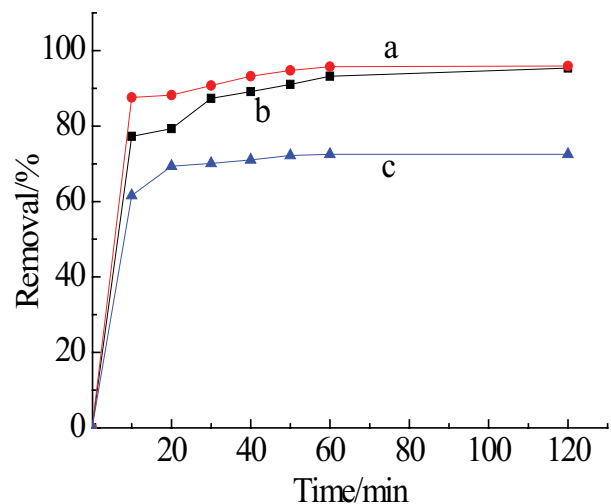


Fig. 8. Removal of phenol in different phenol solution.

with time on PDA/Fe-MOFs/RGO, pseudo-second-order equation [Eq. (6)] was adapted to describe the adsorption of phenol.

$$\frac{t}{q_t} = \frac{1}{kq_e^2} + \frac{t}{q_e} \quad (6)$$

where q_e is the amounts of adsorbate adsorbed at equilibrium and q_t (mg g^{-1}) is the amounts of adsorbate adsorbed at any time t (min). The constant k ($\text{g mg}^{-1} \text{min}^{-1}$) is the adsorption rate constant of pseudo-second-order adsorption. Values of t/q_t are plotted against t as shown in Fig. 9. According to pseudo-second-order model, fitting kinetics parameters of adsorption of phenol on the PDA/Fe-MOFs/RGO are presented in Table 2. According to the R^2 values, it indicated that the pseudo-second-order kinetic model could describe the adsorption process of phenol onto PDA/Fe-MOFs/RGO properly.

Weber and Morris [33] was provided the intraparticle diffusion model, in which the rate for intraparticle diffusion by the relationship between q_t and square root of time $t_{1/2}$ as shown in Eq. (7).

$$q_t = k_{id}t_{1/2} + C_i \quad (7)$$

where k_{id} ($\text{mg g}^{-1} \text{h}^{-0.5}$) is the intraparticle diffusion rate constant and C_i is associated to the boundary layer thickness. According to the intraparticle diffusion model, if q_t vs. $t_{1/2}$ is linear, which proves intraparticle diffusion is occurred, and if the plot passes through the origin, the rate limiting process is only due to the intraparticle diffusion. Otherwise, some other mechanism can also be involved along with intraparticle diffusion. From Fig. 10, it can be seen that q_t vs. $t_{1/2}$ is not linear, implying that the intraparticle diffusion along with surface adsorption was affected by the adsorption of phenol.

3.3. Selectivity study

Competitive adsorption can be used to determine whether imprinted polymers have specific recognition for template molecules. The distribution coefficients K_d and selectivity coefficients k of phenol relative to some interfering molecules are shown in Table 3. As can be seen from Table 3, K_d values of PDA/Fe-MOFs/RGO was higher than the other interfering molecules. In addition, k value of PDA/Fe-MOFs/RGO for methylene blue, *p*-nitrophenol, benzoic acid and hydroquinone are great. These above facts are suggested the adsorption abilities of PDA/Fe-MOFs/RGO for phenol are very strong and far stronger than that for these interfering molecules. The reason was that the cavities imprinted by phenol were non-matched to these interfering molecules,

suggesting that PDA/Fe-MOFs/RGO had good adsorption selectivity for phenol.

3.4. Regeneration of PDA/Fe-MOFs/RGO

Regeneration of PDA/Fe-MOFs/RGO is important in the field of actual application. Desorption of phenol was done

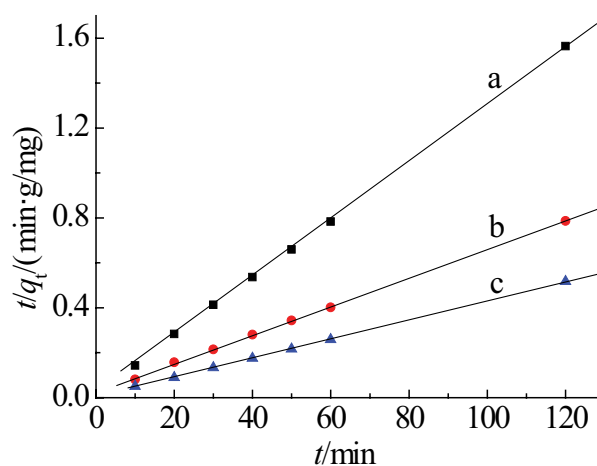


Fig. 9. Plots t/q_t vs. time. (a) 10 mg L^{-1} , (b) 20 mg L^{-1} and (c) 40 mg L^{-1} phenol solutions.

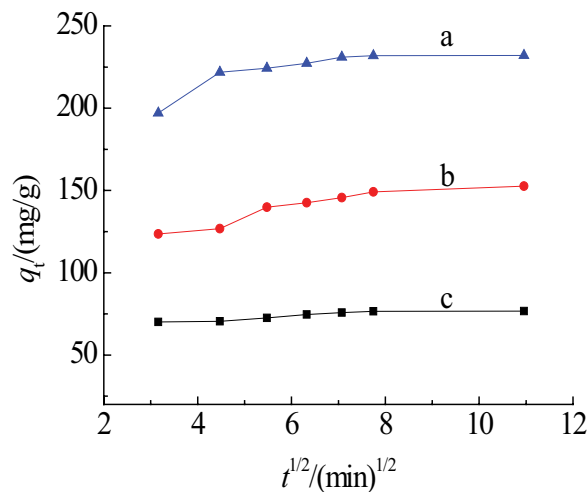


Fig. 10. Intraparticle diffusion plots for the removal of phenol on the PDA/Fe-MOFs/RGO.

Table 2
Fitting kinetics parameters of adsorption of phenol

C_0 (mg L^{-1})	q_e (mg g^{-1})	k ($\text{g mg}^{-1} \text{min}^{-1}$)	R^2
10	77.88	7.95×10^{-3}	0.9999
20	157.48	1.68×10^{-3}	0.9998
40	235.29	3.06×10^{-3}	0.9999

Table 3
Distribution coefficients and selectivity coefficients data

Compounds	K_d	k
Phenol	1,948.05	–
Methylene blue	19.63	99.23
<i>p</i> -nitrophenol	14.03	138.85
Benzoic acid	10.48	185.88
Hydroquinone	16.01	121.68

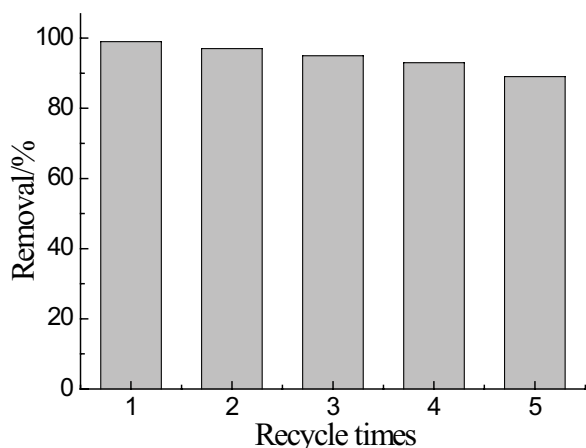


Fig. 11. Cyclic uses of PDA/Fe-MOFs/RGO for the removal of phenol.

by ethanol elution for 2 h. The experimental results are shown in Fig. 11. As seen in Fig. 11, after repeatedly used for 4 times, the removal rate of phenol could still achieve 89%, indicating that PDA/Fe-MOFs/RGO had excellent regeneration performance.

4. Conclusions

A new type of phenol imprinted material, PDA/Fe-MOFs/RGO, was successfully prepared by the surface molecular imprinting technique. The optimum conditions for the selective and high removal of phenol were studied. The results showed that the optimum pH, temperature and adsorbent dose were found 8, 20°C and 125 mg L⁻¹, respectively. Under the optimum conditions, the phenol removal rate was 99.59% containing 20 mg L⁻¹ of phenol. The pseudo-second-order kinetic model was suited for the adsorption process of phenol onto PDA/Fe-MOFs/RGO properly. The intraparticle diffusion along with surface adsorption affected the adsorption of phenol. PDA/Fe-MOFs/RGO also showed excellent adsorption selectivity for phenol and regeneration performance.

Acknowledgments

This work was financially supported by Shaanxi Provincial Natural Science Foundation (No. 2018JM2014, 2019JM-421), Shaanxi Provincial Education Department (No. 2013JK0673), Industrial research project of Science and Technology Department of Shaanxi Province (No. 2017GY-179).

References

- J.M. Pan, H. Hang, X.H. Dai, J.D. Dai, P.W. Huo, Y.S. Yan, Switched recognition and release ability of temperature responsive molecularly imprinted polymers based on magnetic halloysite nanotubes, *J. Mater. Chem.*, 22 (2012) 17167–17175.
- L. Qin, G.M. Zeng, C. Lai, D.L. Huang, P. Xu, C. Zhang, M. Cheng, X.G. Liu, S.Y. Liu, B.H. Li, H. Yi, “Gold rush” in modern science: fabrication strategies and typical advanced applications of gold nanoparticles in sensing, *Coord. Chem. Rev.*, 359 (2018) 1–31.
- S.F. Raof, S. Mohamad, M.R. Abas, Synthesis and evaluation of molecularly imprinted silica gel for 2-hydroxybenzoic acid in aqueous solution, *Int. J. Mol. Sci.*, 14 (2013) 5952–5965.
- G. Wulff, Enzyme-like catalysis by molecularly imprinted polymers, *Chem. Rev.*, 102 (2001) 1–28.
- L. Feng, Y.J. Liu, Y.Y. Tan, J. Hu, Biosensor for the determination of sorbitol based on molecularly imprinted electrosynthesized polymers, *Biosens. Bioelectron.*, 19 (2004) 1513–1519.
- N. Tancredi, N. Medero, F. Möller, J. Piriz, C. Plada, T. Cordero, Phenol adsorption onto powdered and granular activated carbon, prepared from *Eucalyptus* wood, *J. Colloid Interface Sci.*, 279 (2004) 357–363.
- L. Qin, G.M. Zeng, C. Lai, D.L. Huang, C. Zhang, P. Xu, T.J. Hu, X.G. Liu, M. Cheng, Y. Liu, L. Hu, Y.Y. Zhou, A visual application of gold nanoparticles: simple, reliable and sensitive detection of kanamycin based on hydrogen-bonding recognition, *Sens. Actuators, B*, 243 (2017) 946–954.
- D.A. Spivak, K.J. Shea, Investigation into the scope and limitations of molecular imprinting with DNA molecules, *Anal. Chim. Acta*, 435 (2001) 65–74.
- W.M. Xuan, C.F. Zhu, Y. Liu, Y. Cui, Mesoporous metal–organic framework materials, *Chem. Soc. Rev.*, 41 (2012) 1677–1695.
- X.D. Zhao, D.H. Liu, H.L. Huang, W.J. Zhang, Q.Y. Yang, C.G. Zhong, The stability and defluorination performance of MOFs in fluoride solutions, *Microporous Mesoporous Mater.*, 185 (2014) 72–78.
- H. Su, Y. Lin, Z. Wang, Y.L. Wong, X. Chen, T.W. Chan, Magnetic metal-organic framework-titanium dioxide nanocomposite as adsorbent in the magnetic solid-phase extraction of fungicides from environmental water samples, *J. Chromatogr. A*, 1466 (2016) 21–28.
- K. Qian, G.Z. Fang, S. Wang, A novel core–shell molecularly imprinted polymer based on metal–organic frameworks as a matrix, *Chem. Commun.*, 47 (2011) 10118–10120.
- H.L. Liu, L. Mu, X.M. Chen, J. Wang, S. Wang, B.G. Sun, Core–shell metal–organic frameworks/molecularly imprinted nanoparticles as absorbents for the detection of pyrroline in milk and milk powder, *J. Agric. Food Chem.*, 65 (2017) 986–992.
- J.J. Fan, S.W. Liu, J.G. Yu, Enhanced photovoltaic performance of dye-sensitized solar cells based on TiO₂ nanosheets/graphene composite films, *J. Mater. Chem.*, 22 (2012) 17027–17036.
- Z.J. Wei, R.F. Pan, Y.X. Hou, Y. Yang, Y.X. Liu, Graphene-supported Pd catalyst for highly selective hydrogenation of resorcinol to 1,3-cyclohexanedione through giant π -conjugate interactions, *Sci. Rep.*, 5 (2015) 15664.
- C. Petit, B. Levasseur, B. Mendoza, T.J. Bandoz, Reactive adsorption of acidic gases on MOF/graphite oxide composites, *Microporous Mesoporous Mater.*, 154 (2012) 107–112.
- L. Li, X.L. Liu, H.Y. Geng, B. Hu, G.W. Song, Z.S. Xu, The MOF/graphite oxide hybrid (MOFs: (Cu₃(BTC)₂(H₂O)₃) materials for the adsorption of methylene blue from aqueous solution, *J. Mater. Chem. A*, 1 (2013) 10292–10299.
- L. Li, Z. Shi, H. Zhu, W. Hong, F. Xie, K. Sun, Adsorption of azo dyes from aqueous solution by the hybrid MOFs/GO, *Water Sci. Technol.*, 73 (2016) 1728–1737.
- W.S. Hummers Jr., R.E. Offeman, Preparation of graphitic oxide, *J. Am. Chem. Soc.*, 80 (1958) 1339.
- Y. Jin, C.C. Zhao, Z. Sun, Y.C. Lin, L. Chen, D. Wang, C. Shen, Facile synthesis of Fe-MOF/RGO and its application as a high performance anode in lithium-ion batteries, *RSC Adv.*, 6 (2016) 30763–30768.
- F.Q. An, B.J. Gao, Adsorption characteristics of Cr(III) ionic imprinting polyamine on silica gel surface, *Desalination*, 249 (2009) 1390–1396.
- S.-H. Park, S.-M. Bak, K.-H. Kim, J.-P. Jegal, S.-I. Lee, J.H. Lee, K.-B. Kim, Solid-state microwave irradiation synthesis of high quality graphene nanosheets under hydrogen containing atmosphere, *J. Mater. Chem.*, 21 (2011) 680–686.
- M.J. Fernández-Merino, L. Guardia, J.I. Paredes, S. Villar-Rodil, P. Solís-Fernández, A. Martínez-Alonso, J.M.D. Tascón, Vitamin C is an ideal substitute for hydrazine in the reduction of graphene oxide suspensions, *J. Phys. Chem. C*, 114 (2010) 6426–6432.

- [24] W.J. Si, X.Z. Wu, J. Zhou, F.F. Guo, S.P. Zhuo, H.Y. Cui, W. Xing, Reduced graphene oxide aerogel with high-rate supercapacitive performance in aqueous electrolytes, *Nanoscale Res. Lett.*, 8 (2013) 247.
- [25] Y. Cong, T. Xia, M. Zou, Z. Li, B. Peng, D.Z. Guo, Z.W. Deng, Mussel-inspired polydopamine coating as a versatile platform for synthesizing polystyrene/Ag nanocomposite particles with enhanced antibacterial activities, *J. Mater. Chem. B*, 2 (2014) 3450–3461.
- [26] N. Wei, Y.Y. Jiang, Y. Ying, X.Y. Guo, Y.P. Wu, Y. Wen, H.F. Yang, Facile construction of a polydopamine-based hydrophobic surface for protection of metals against corrosion, *RSC Adv.*, 7 (2017) 11528–11536.
- [27] S. Leng, T. Wang, M. Yang, Y. Zhao, W.Q. Lu, R.M. Wang, G.Y. Sun, Preparation and electrochemical performance of nitrogen doped carbon materials based on polydopamine, *Chin. J. Appl. Chem.*, 35 (2018) 477–483.
- [28] V. Jabbari, J.M. Veleta, M. Zarei-Chaleshtori, J. Gardea-Torresdey, D. Villagrán, Green synthesis of magnetic MOF@GO and MOF@CNT hybrid nanocomposites with high adsorption capacity towards organic pollutants, *Chem. Eng. J.*, 304 (2016) 774–783.
- [29] A.R. Iftikhar, H.N. Bhatti, M.A. Hanif, R. Nadeem, Kinetic and thermodynamic aspects of Cu(II) and Cr(III) removal from aqueous solutions using rose waste biomass, *J. Hazard. Mater.*, 161 (2009) 941–947.
- [30] K. Saltalı, A. Sari, M. Aydın, Removal of ammonium ion from aqueous solution by natural Turkish (Yıldızeli) zeolite for environmental quality, *J. Hazard. Mater.*, 189 (2007) 258–263.
- [31] M. Kilic, E. Apaydin-Varol, A.E. Pütün, Adsorptive removal of phenol from aqueous solutions on activated carbon prepared from tobacco residues: equilibrium, kinetics and thermodynamics, *J. Hazard. Mater.*, 189 (2011) 397–403.
- [32] N. Singh, C. Balomajumder, Simultaneous removal of phenol and cyanide from aqueous solution by adsorption onto surface modified activated carbon prepared from coconut shell, *J. Water Process Eng.*, 9 (2016) 233–245.
- [33] W.J. Weber, J.C. Morris, Kinetics of adsorption on carbon from solution, *J. Sanitary Eng. Div.*, 89 (1963) 53–61.